Transport and Communications Science Journal, Vol. 77, Issue 09 (11/2026), 1185-1197

Transport and Communications Science Journal

A PROBABILISTIC MACHINE LEARNING FRAMEWORK OF FLUTTER CRITICAL WIND VELOCITY PREDICTION FOR CABLE-STAYED BRIDGES BASED ON A CALIBRATED FINITE ELEMENT MODEL

Ho Xuan Nam*, Nguyen Ngoc Lan

Application of Artificial Intelligence for Structural Health Monitoring (AI-SHM) Research Group (R2026-UTC-01), Faculty of Civil and Environmental Engineering, University of Transport and Communications, Hanoi, Vietnam

ARTICLE INFO

TYPE: Research Article
Received: 25/09/2026
Revised: 02/11/2026
Accepted: 09/11/2026
Published online: 15/11/2026
https://doi.org/10.47869/tcsj.77.9.5
* *Corresponding author*
Email: hxnam@utc.edu.vn; Tel: 0978918968

Abstract. Flutter is a self-excited aeroelastic instability that controls the wind design of long-span cable-stayed bridges. It is usually assessed by wind tunnel tests or costly simulations. This study examines whether a probabilistic machine learning model can give a first estimate of the flutter critical wind velocity, based on flat-plate theory, from preliminary design parameters, for a family of bridges derived from one existing bridge. A finite element model of the Dakrong cable-stayed bridge in Vietnam is updated to match ten of the twelve natural frequencies measured on site (root-mean-square error 4.7%). Three hundred bridge configurations are generated from the updated model by Latin Hypercube Sampling of eleven variables within slenderness limits, and their critical velocity is estimated with the Selberg formula and checked with the Rocard formula. On a test set of 61 configurations, Gaussian process regression with automatic relevance determination, trained only on span, width, depth, mass and inertia, reproduces the Selberg estimate with R^2 = 0.92 and a mean absolute percentage error of 6.4%, and 95.1% of the test values fall inside its 95% confidence intervals. These values measure agreement with the formula-based labels, not with the actual flutter speed. The labels assume flat-plate aerodynamics and a single pair of modes, and additional checks suggest that, for this open-girder deck, their uncertainty is larger than the prediction error. The model is therefore intended only for comparing deck alternatives within the sampled family and does not replace a flutter check.

Keywords: flutter instability, cable-stayed bridge, critical wind velocity, Gaussian process regression, finite element model updating, machine learning.

© 2026 University of Transport and Communications

1. INTRODUCTION

Long-span cable-supported bridges are becoming more flexible and lighter, so they are more sensitive to wind effects such as vortex shedding, buffeting, galloping, and flutter [1]. Flutter is the most dangerous of these. It is a self-excited instability: the vertical bending and the torsion of the deck are coupled, the coupled motion takes energy from the wind, and the oscillations grow exponentially once the wind speed exceeds a critical value. The collapse of the original Tacoma Narrows Bridge in 1940 is the best-known example. Checking that a bridge has a sufficient margin against flutter is now a standard part of the wind design of long-span bridges [1, 2].

The critical wind velocity for flutter is usually obtained either from section model tests in a wind tunnel [3, 4] or from aeroelastic analyses that use flutter derivatives [2]. Both methods are accurate but costly. Wind tunnel tests need special facilities and several weeks of work, and computational fluid dynamics and coupled flutter analyses need fine meshes, turbulence models and considerable expertise. Simple closed-form formulas, such as those of Selberg [5] and Rocard [6], are therefore still widely used for early checks. These formulas treat the deck like a flat plate and are based on Theodorsen's unsteady aerodynamic theory [7]; they are used because full analyses are not practical at the early design stage [8]. Even these formulas, however, need the fundamental vertical bending and torsional frequencies, and these frequencies can only be obtained from a full dynamic analysis of the structure.

In recent years, machine learning (ML) and deep learning have been widely applied in wind and structural engineering. Examples include predicting the flutter velocity of suspension bridges from their structural properties [9], detecting damage in cable-stayed bridges from vibration data [10], structural health monitoring with advanced network architectures [11], and detecting damage in steel truss bridges from augmented time-series data [12]. These studies show that data-driven surrogate models can approximate costly analyses at a low computational cost, as long as they are used within the range of their training data. Methods that account for uncertainty are also not new in bridge aeroelasticity. Random eigenvalue analyses have been used to estimate the probability of flutter of long-span bridges when the modal and aerodynamic parameters are uncertain [13], and Bayesian neural networks have been used to monitor a cable-stayed bridge so that each prediction comes with its own confidence level [14]. Two limitations of existing surrogate models led to the present study. First, most published surrogate models of the flutter velocity are deterministic: they give a single value and do not say how uncertain it is, which is hard to accept when the predicted value is used in a safety check. Second, the training data are usually collected from different published sources measured under different conditions, and the structural models behind them are rarely checked against field measurements on a real bridge.

In Vietnam, more and more cable-stayed bridges with main spans of 150-350 m are in service or under construction, but there are few wind tunnel facilities. A method that estimates the flutter critical velocity at the first sizing of the deck, and that reports its own uncertainty, could help at that stage, provided that its assumptions and range of validity are clearly understood.

This paper is a first step in this direction for one family of bridges. It has three parts. (i) A finite element (FE) model of the Dakrong cable-stayed bridge is updated to match ten of the twelve natural frequencies measured on site. The updating uses differential evolution with parameter bounds that are physically reasonable. The updated model matches the measured

deck frequencies with a root-mean-square error of 4.7%. (ii) A family of 300 bridge configurations is generated from the updated model by Latin Hypercube Sampling under given constraints. Each configuration is labelled with the critical velocity given by the Selberg formula and checked with the Rocard formula; both formulas were first checked against published results for the Great Belt East Bridge. (iii) A surrogate model based on Gaussian process regression (GPR) with automatic relevance determination (ARD) is trained to predict the Selberg estimate from design parameters only, and we check how often the reference values fall inside its 95% confidence intervals. The labels come from closed-form formulas, and the limitations that result from this choice are discussed in detail in Section 5.

The paper is organized as follows. Section 2 summarizes the flutter problem and the closed-form formulas used. Section 3 describes the FE model, how it was updated against the field measurements, and how the database was generated. Section 4 presents the machine learning models and how they were evaluated. Section 5 presents and discusses the results, and the last section gives the conclusions.

2. CLOSED-FORM ESTIMATES OF THE FLUTTER CRITICAL VELOCITY

In the classical two-degree-of-freedom model of flutter, the vertical displacement h and the torsional rotation α of the deck section are coupled. For a thin flat plate in smooth flow, the self-excited lift and moment are given exactly by Theodorsen's circulation function [7], and the critical state is found by solving the complex eigenvalue problem of the coupled system [1]. For bridge decks, the aerodynamic coefficients are replaced by flutter derivatives measured in wind tunnel tests [2]. At the preliminary design stage these derivatives are not available, so closed-form formulas fitted to the flat-plate solution are commonly used [8].

Selberg's formula [5] gives the flutter critical wind velocity of a streamlined deck as

$$U_{\mathrm{cr}} \;=\; 3.72\, B\, f_{\alpha} \sqrt{\frac{m\, r}{\rho B^{3}}\left[1 \;-\; \left(\frac{f_h}{f_{\alpha}}\right)^{2}\right]} \tag{1}$$

where B is the total deck width, f_α and f_h are the fundamental torsional and vertical bending frequencies (Hz), m and I_m are the mass and the mass moment of inertia of the deck per unit length, $r = (I_m/m)^{1/2}$ is the radius of gyration, and ρ is the air density. Rocard's formula [6], in the form used in [15], gives a second, independent estimate of the same kind:

$$U_{\mathrm{cr}} \;=\; 0.443 \;\cdot\; 2\pi\, f_{\alpha}\, B \sqrt{\frac{\left(1 - \left(\frac{f_h}{f_{\alpha}}\right)^{2}\right)}{\mu} \;\cdot\; \frac{2\nu}{1+\nu}} \tag{2}$$

where $\mu = \pi\rho B^2/(2m)$ is the ratio of air mass to structural mass and $\nu = 8I_m/(B^2 m)$ is a dimensionless inertia ratio. Both formulas assume flat-plate aerodynamics and bending and torsional frequencies that are well apart; they are no longer valid when f_h comes close to f_α [8].

Our implementation of Eqs. (1) and (2) was checked on the Great Belt East Bridge (B = 31 m, m = 22.7 t/m, $I_m = 2.47\times10^6$ kg·m²/m, f_h = 0.099 Hz, f_α = 0.278 Hz). With the air density of 1.225 kg/m³ used for all labels, the two formulas give 76.3 and 76.6 m/s, which are of the same order as the flutter limit found for this bridge in its final aerodynamic design [3]. The implementation was also compared with an open-source frequency-domain flutter program that reports the Selberg and Rocard estimates together with its own coupled solution [15]. In this study Eq. (1) gives the reference labels for machine learning, and Eq. (2) is used as an

independent check; its difference from Eq. (1) gives part of the label uncertainty. Both formulas also assume smooth incoming flow. Time-domain simulations of long-span bridges show that atmospheric turbulence makes the bridge more stable: it raises the critical velocity by about 5 to 10% when the turbulence intensity is high (15 to 20%), and hardly changes it at typical intensities of 5 to 10% [16]. In this respect only, the labels used here are on the safe side; for bluff decks, the flat-plate assumption itself may have the opposite effect, as discussed in Section 5. Note also that the finite element model contains no aerodynamic forces: the self-excited forces enter only through the closed-form section-model formulas.

3. CALIBRATED FINITE ELEMENT MODEL AND DATABASE GENERATION

3.1. The Dakrong bridge and its finite element model

The Dakrong bridge is a cable-stayed bridge on National Highway 9 in Quang Tri province, Vietnam. The deck is 173.9 m long and 9.0 m wide (an 8.0 m carriageway and two 0.5 m strips). It is a composite deck made of two steel I-girders 1.024 m deep and 7.0 m apart, cross-beams, and a reinforced concrete slab 150 mm thick. It is carried by fifteen pairs of stay cables anchored to a single reinforced concrete pylon. A three-dimensional FE model of the bridge (Figure 1) was built in ANSYS, using BEAM188 elements for the girders, cross-beams and pylon, LINK-type elements for the stay cables, and SHELL181 elements for the deck slab; the model has 306 nodes and 499 elements.

In September 2022, an ambient vibration test was carried out on the bridge, with piezoelectric accelerometers placed in several setups along both edges of the deck. Operational modal analysis, which is now the usual way to obtain the modal parameters of cable-stayed bridges under ambient excitation [17], gave twelve natural frequencies of deck modes between 1.00 Hz and 7.65 Hz. These frequencies are used here as the target for model updating. Details of the test are given in the bridge inspection report and follow earlier dynamic tests by the group [18].

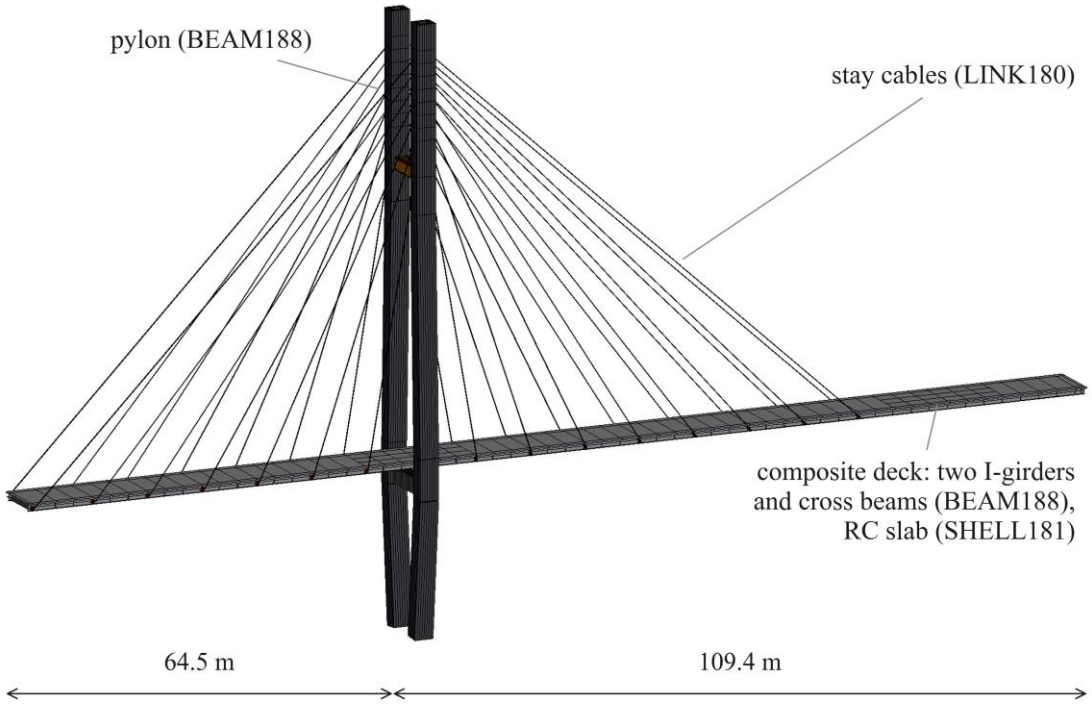


Figure 1. Finite element model of the Dakrong cable-stayed bridge.

3.2. Model updating against field measurements

Five parameters were updated: a multiplier on the steel modulus, the concrete modulus of the pylon, the equivalent slab modulus, a multiplier on the cable area, and a multiplier on the mass density. Their bounds (Table 1) were limited to physically reasonable ranges. A run without bounds reached a slightly lower frequency error (4.0% compared with 4.7%), but it gave a steel modulus of 240 GPa and a cable area reduced by 40%, which are not physically realistic. These values show that the parameters were compensating for errors in the model itself rather than correcting the real material and section properties. The bounded problem was solved by differential evolution [19] with 417 runs of the FE model, minimizing the root-mean-square relative difference between the first ten model frequencies of deck modes and the measured ones.

The model and measured frequencies were paired in increasing order of the deck modes. Figure 2 compares the measured and updated frequencies: nine of the ten pairs agree within ±10%, the RMS error is 4.68%, and only the first mode differs by +11.8%. The cable-area and mass multipliers ended near their bounds. This suggests that the main remaining model error is that the linear modal analysis does not include the stiffening caused by cable pretension.

Table 1. Updating variables, physically admissible bounds, and identified values.

Variable	Lower	Upper	Identified
Steel modulus multiplier (-)	0.95	1.05	0.998
Pylon concrete modulus (GPa)	28	38	30.7
Equivalent slab modulus (GPa)	2	35	3.78
Cable area multiplier (-)	0.85	1.15	0.861
Mass density multiplier (-)	0.95	1.10	1.094

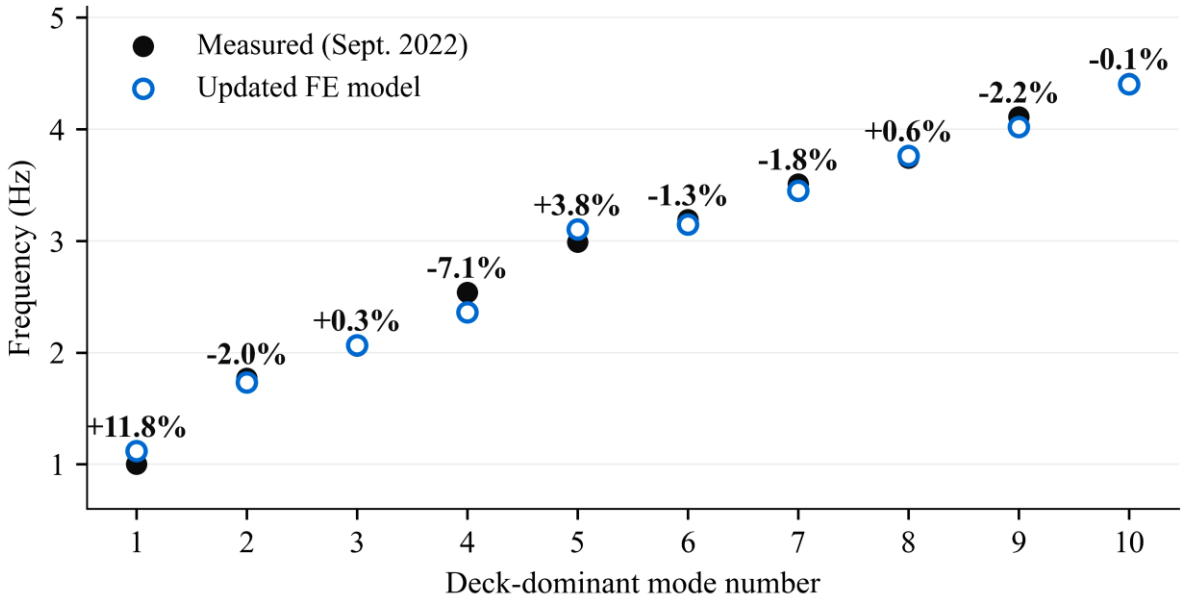


Figure 2. Measured and updated model frequencies of the ten deck-dominant modes.

3.3. Parametric database and flutter labels

A family of bridge configurations was created from the updated model by scaling eleven design variables (Table 2). These are: a span scale factor applied to the longitudinal and vertical coordinates (so that the ratio of pylon height to span is kept), a width scale factor applied to the transverse coordinates, multipliers on the elastic moduli and density, the cable area, the girder depth and flange width, the slab thickness, and the damping ratio (recorded for completeness, although Eqs. (1)-(2) do not use damping). Samples were drawn by Latin Hypercube Sampling [20] and kept only if they met two slenderness limits: a width-to-depth ratio $3.8 \leq B/D \leq 15.4$ and a span-to-depth ratio $110 \leq L/D \leq 240$, the latter centred on the value $L/D = 170$ of the existing bridge. The 300 accepted samples have total lengths of 174-340 m, deck widths of 6.3-14.4 m and deck masses of 4.1-14.7 t/m (Figure 3); this range overlaps with that of medium-span cable-stayed bridges in Vietnam.

Table 2. Design variables of the parametric family.

Variable	Range	Variable	Range
Span scale factor	1.0-2.0	Girder depth mult.	0.7-1.8
Width scale factor	0.7-1.6	Flange width mult.	0.8-1.3
Steel modulus mult.	0.9-1.1	Slab thickness mult.	1.0-2.5
Concrete modulus mult.	0.9-1.1	Cable area mult.	0.75-1.25
Cable modulus mult.	0.9-1.1	Damping ratio	0.3-1.0%
Density mult.	0.95-1.05	Constraints	*B/D 3.8-15.4; L/D 110-240*

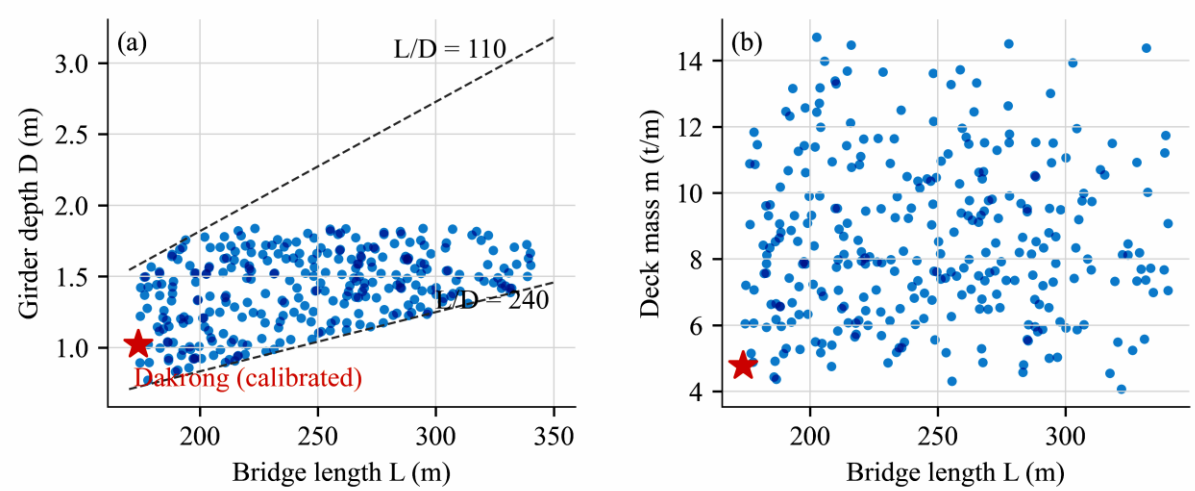


Figure 3. Coverage of the parametric family. (a) Girder depth versus length with slenderness bounds. (b) Deck mass versus length.

Each configuration was analysed in ANSYS in batch mode, which took about three seconds per modal analysis (301 runs including the baseline). The vertical bending and torsional modes were identified automatically from the vertical displacements of the sixty-one pairs of nodes on the two deck edges. The correlation coefficient between the displacements of the two edges is +1 for bending and −1 for torsion (Figure 4), and modes whose deck amplitude is less than 10%

of the maximum (modes dominated by the pylon) are ignored. A bending mode and a torsional mode were found in all 301 runs. In 15 configurations, however, all longer than 265 m, the first antisymmetric mode taken as the torsional mode has a deck amplitude of only 10.6-13.7% of the largest deck amplitude. This is close to the 10% limit, and the mode is probably dominated by the pylon. These configurations give the lowest labels (38-66 m/s), and their effect is examined in Section 5. The deck mass and mass moment of inertia per unit length were computed from the deck elements only, without the pylon and cables, by summing the element masses and their parallel-axis terms about the centre of mass of the deck.

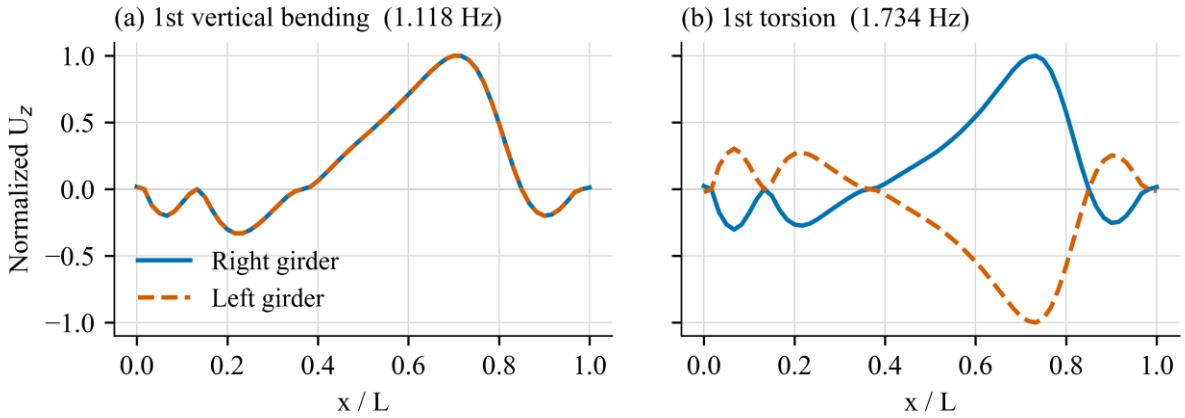


Figure 4. Automatic mode classification from edge deflection profiles of the baseline model. (a) First vertical bending. (b) First torsion.

Applying Eq. (1) to the 300 configurations gives critical velocities between 38 and 189 m/s (Figure 5a). The Rocard estimate differs from the Selberg label by 3.0% on average and by at most 3.7% (Figure 5b). Since both formulas are based on the same flat-plate assumptions, this difference is only a lower bound of the label uncertainty (Section 5).

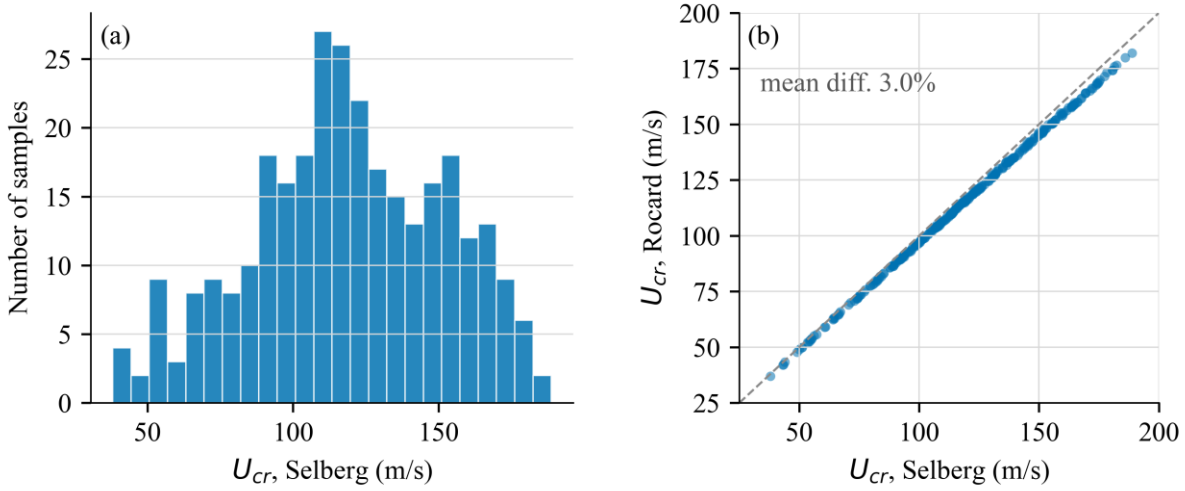


Figure 5. Flutter labels of the database. (a) Distribution of the Selberg critical velocity. (b) Cross-check against the Rocard estimate.

4. PROBABILISTIC MACHINE LEARNING MODELS

Gaussian process regression [21] assumes a Gaussian prior over functions. For each input it returns a Gaussian distribution: its mean is the prediction and its standard deviation measures the uncertainty of that prediction. We used a Matérn 5/2 kernel with automatic relevance determination, in which each input has its own length-scale. After training, a shorter length-scale means a more influential input, so the regression also ranks the inputs by importance. A white-noise term was added, and all hyperparameters were found by maximizing the log-marginal likelihood with three restarts. Random forest [22], XGBoost [23] and a neural network with two hidden layers (64-32 neurons) were used as deterministic models for comparison, all implemented in scikit-learn [24].

Two sets of inputs are used. In the full scenario, the inputs include the modal frequencies f_h and f_α. Because the label from Eq. (1) is an algebraic function of (B, m, I_m, f_h, f_α), this scenario only interpolates a smooth known surface, and its almost perfect accuracy ($R^2 \approx 1.00$) is reported only as an internal check. It is also used for a noise study, in which Gaussian noise of 2% and 3% is added to both frequencies; this range is our assumption for the scatter of frequencies identified by operational modal analysis. In the design scenario, which is the one of practical interest, the inputs are only quantities known at the preliminary design stage: L, B, D, B/D, m and I_m. The model must then learn, without being told, both the dynamic behaviour of the bridge family and the aerodynamic formula, and no dynamic analysis is needed to make a prediction.

The data were split into a training set (80%) and a test set (20%) with a fixed random seed, and five-fold cross-validation on the training set was used to check that the model ranking is stable. Accuracy on the test set is reported by the coefficient of determination R^2, the root-mean-square error, the mean absolute error and the mean absolute percentage error (MAPE). The quality of the GPR uncertainty is checked by the share of test values that fall inside its 95% confidence intervals (empirical coverage).

5. RESULTS AND DISCUSSION

Table 3 gives the test-set results of the four models in the design scenario. GPR is the most accurate on this test set ($R^2 = 0.919$, MAPE = 6.4%), followed by the neural network (0.903, 7.2%), XGBoost (0.892, 9.1%) and random forest (0.878, 9.0%). The cross-validation averages also rank GPR first, although XGBoost and random forest swap places (Figure 7), and the differences between the models are small. Figure 6 shows the GPR predictions against the reference values with their 95% confidence intervals. Most points lie close to the diagonal over the range of 38-189 m/s, and three reference values fall outside the predicted intervals. The share of test values inside the 95% intervals is 95.1% for this single split of 61 test samples; averaged over ten random splits it is 97.9%, so at this level the intervals tend to be somewhat too wide rather than too narrow. The accuracy is not the same everywhere. For configurations longer than 290 m, the MAPE rises to 22.4% and the coverage falls to 70% (10 test samples). Most of this error comes from the 15 configurations with an unclear torsional mode (Section 3.3). When they are removed and the remaining 286 configurations are split in the same way, GPR reaches $R^2 = 0.965$ and MAPE = 3.3%; when their labels are recomputed with the next torsional mode, which is dominated by the deck, R^2 drops to 0.54. The largest errors therefore occur in the long-span part of the family, which is also where the critical velocities are lowest.

Table 3. Test-set performance in the design scenario (inputs: L, B, D, B/D, m, I_m).

Model	R^2	RMSE (m/s)	MAE (m/s)	MAPE (%)	CV R^2 (5-fold)
GPR (Matérn 5/2 + ARD)	0.919	10.20	5.69	6.43	0.926 ± 0.072
ANN (64-32)	0.903	11.12	6.64	7.15	0.908 ± 0.074
XGBoost	0.892	11.79	8.19	9.14	0.887 ± 0.057
Random forest	0.878	12.52	8.50	8.98	0.890 ± 0.059

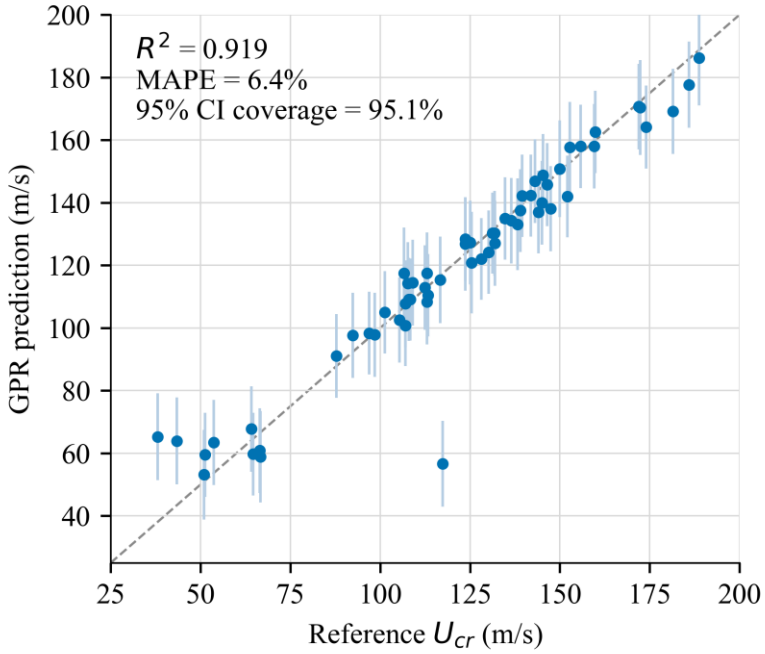


Figure 6. GPR predictions with 95% confidence intervals against reference values (design scenario, test set).

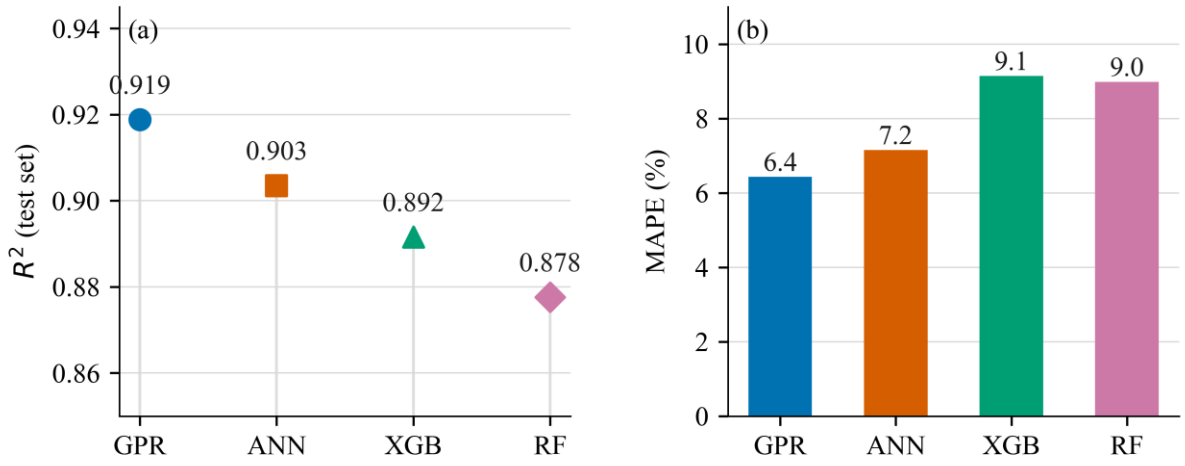


Figure 7. Comparison of the four surrogate models on the test set. (a) Coefficient of determination. (b) Mean absolute percentage error.

The ARD length-scales of the design-scenario GPR (Figure 8) show that, within this family, the deck width B, the length L and the mass m have the most influence. D has a weak influence, and B/D and I_m are in practice not used. This does not mean that I_m has no physical effect. Within the generated family the ratio 2r/B varies only between 0.47 and 0.53, so I_m gives almost no information beyond m and B. In the full scenario, the ARD keeps I_m, B, m, the frequency ratio and f_α, and drops L, D and the damping ratio; these are the variables that appear in Eq. (1).

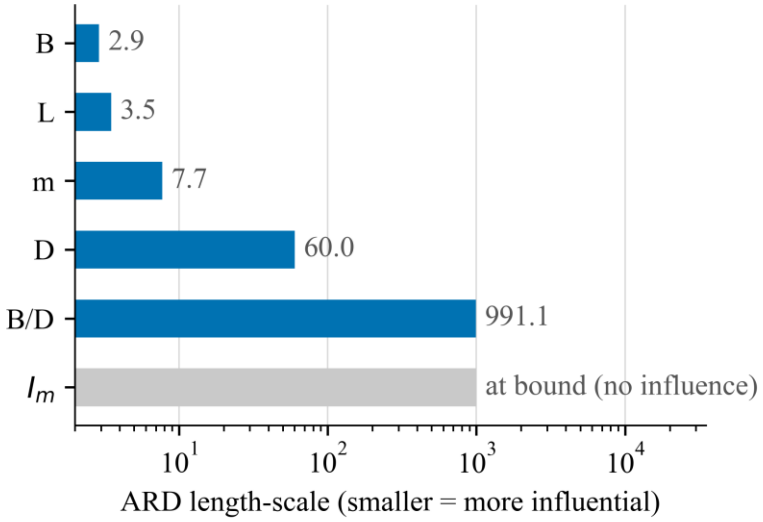


Figure 8. ARD length-scales of the design-scenario GPR; smaller values indicate more influential inputs.

The noise study (Figure 9) shows how sensitive the full-scenario models are to noise in the frequency inputs. With 2% and 3% Gaussian noise on both frequencies, GPR keeps $R^2 = 0.993$ and 0.989, respectively, and stays above the tree-based models. Because the noise is artificial, these results do not replace a test with frequencies identified on real bridges. The design scenario is not affected, because it uses no frequency input.

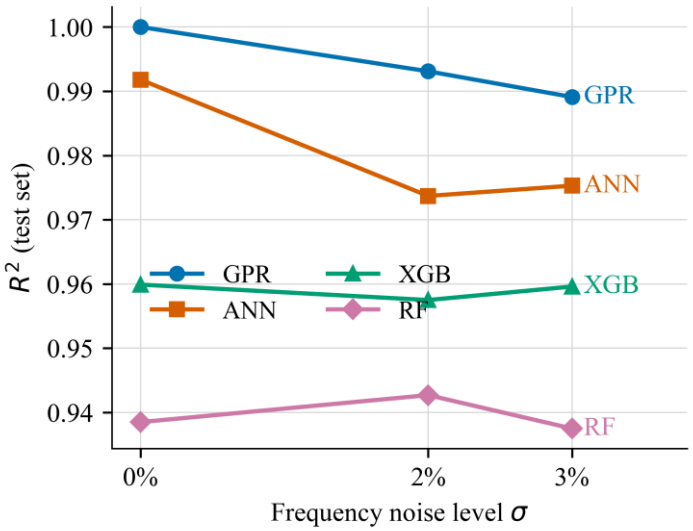


Figure 9. Sensitivity of the full-scenario models to Gaussian noise on the modal frequencies.

The results have several limitations:

(i) Labels from closed-form formulas. The labels are Selberg estimates, which assume flat-plate aerodynamics in smooth flow and a single pair of bending and torsional modes. They are not measured or computed flutter speeds, and the accuracy values in Section 5 only show how well the model reproduces these estimates. The 3.0% average difference from the Rocard estimate is a lower bound of the label uncertainty, because both formulas use the same assumptions. Free-stream turbulence [16] and deck details such as railings and barriers [4] are not included.

(ii) Modal mass of the torsional mode. Eqs. (1)-(2) assign the whole deck mass and inertia to the mode identified as torsional. Because the exported modes are normalized to the mass of the whole structure, we could compute afterwards how much of their kinetic energy is in the deck. For the mode used as f_α, this share is only 0.5-19% across the family (median 8.7%; 7.7% for the baseline bridge); the rest is in the cables, the pylon and the lateral motion of the deck. The closed-form formulas therefore do not represent the generalized mass of this mode. The 15 configurations with an unclear torsional mode are one visible result of this. A multimode analysis [25] would avoid choosing a single mode.

(iii) Aerodynamics of the open section. The Dakrong deck has two open I-girders. Such bluff sections are prone to torsional flutter, which flat-plate theory cannot describe because in that theory the torsional damping derivative A_2^* is always negative. After this study, preliminary two-dimensional CFD simulations of the deck section in forced vibration were carried out following [26], without railings and without a mesh-independence check. They gave a positive A_2^* above $U/(fB) \approx 6$. When these derivatives were used in a multimode analysis with the first twenty modes, the baseline bridge gave about 120 m/s instead of 153.7 m/s, and the whole family gave 0.44-1.76 times the Selberg estimates, with a correlation of 0.76 between the two. These preliminary results are not used in this paper and still need to be checked by experiments. They suggest, however, that for this type of deck the label uncertainty may be several tens of percent, larger than the 6.4% prediction error of the model, and that the flat-plate labels are not necessarily on the safe side. The label of the baseline bridge should not be taken as its predicted flutter speed.

(iv) Structural model. The modal analyses are linear and do not include the stiffening caused by cable pretension. The updated parameters partly compensate for this model error, as the cable-area and mass multipliers ending near their bounds suggest. Model and measured modes were paired by their order, because the measured mode shapes were not available in digital form for a modal assurance criterion. The deck mass used in Eqs. (1)-(2) does not include the cables.

(v) Data and evaluation. All configurations are derived from a single reference bridge by limited scaling. The model should therefore not be used for other deck types, other cable layouts or two-pylon bridges, and the slenderness limits $L/D \in [110, 240]$ have not been compared with data on existing bridges. The test set has 61 samples, and only ten of them are in the long-span part of the family, where the errors are largest. The confidence intervals describe the uncertainty of the model relative to the labels, not the uncertainty of the labels or of the FE model.

For these reasons, the procedure is intended for comparing deck alternatives within the sampled family, not for predicting flutter. The next steps are wind tunnel tests or validated CFD of the actual deck section, multimode flutter analyses with flutter derivatives of that section, modal analyses that include cable pretension, and digitized measured mode shapes.

6. CONCLUSION

This paper presented a probabilistic machine learning procedure for estimating the flutter critical wind velocity of a family of cable-stayed bridges. The family was derived from a finite element model of the Dakrong bridge updated against field measurements. Within the limitations given in Section 5, the main findings are: (1) model updating with physically reasonable parameter bounds matched ten measured deck frequencies with an RMS error of 4.68%, whereas updating without bounds reached 4.0% only with unrealistic parameter values; (2) the family of 300 configurations, with lengths of 174-340 m, gave Selberg estimates of 38-189 m/s, which differ from the Rocard estimates by 3.0% on average; (3) Gaussian process regression trained only on design parameters reproduced the Selberg estimate with $R^2 = 0.92$ and MAPE = 6.4% on the test set, slightly better than the ANN, XGBoost and random forest models tested, and its error rises to about 22% for spans above 290 m; and (4) 95.1% of the test values fell inside its 95% confidence intervals. The labels are flat-plate estimates, and for open-girder decks their uncertainty appears to be larger than the prediction error of the model. The results can therefore be used only to compare deck alternatives within the sampled family; they do not replace a flutter check based on flutter derivatives of the actual section or on wind tunnel tests.

ACKNOWLEDGMENT

This research was funded by the University of Transport and Communications (UTC) under grant number T2025-CT-008TD.

REFERENCES

[1]. E. Simiu, R. H. Scanlan, Wind Effects on Structures: Fundamentals and Applications to Design, 3rd ed., John Wiley & Sons, New York, 1996.

[2]. R. H. Scanlan, J. J. Tomko, Airfoil and bridge deck flutter derivatives, Journal of the Engineering Mechanics Division, 97 (1971) 1717-1737. https://doi.org/10.1061/JMCEA3.0001526

[3]. A. Larsen, Aerodynamic aspects of the final design of the 1624 m suspension bridge across the Great Belt, Journal of Wind Engineering and Industrial Aerodynamics, 48 (1993) 261-285. https://doi.org/10.1016/0167-6105(93)90141-A

[4]. E. López-Núñez, M. Ogueta-Gutiérrez, O. Gómez-Ortega, R. Manzanares-Bercial, E. Roibás-Millán, S. Franchini, Effect of wind barriers on the aeroelastic instabilities of a hinged-deck cross-section cable-stayed bridge, Engineering Structures, 287 (2023) 116112. https://doi.org/10.1016/j.engstruct.2023.116112

[5]. A. Selberg, Oscillation and aerodynamic stability of suspension bridges, Acta Polytechnica Scandinavica, Civil Engineering and Building Construction Series No. 13, Trondheim, 1961.

[6]. Y. Rocard, Instabilité des ponts suspendus dans le vent - expériences sur modèle réduit, National Physical Laboratory Paper No. 10, 1963.

[7]. T. Theodorsen, General theory of aerodynamic instability and the mechanism of flutter, NACA Report No. 496, National Advisory Committee for Aeronautics, 1935.

[8]. T. Abbas, I. Kavrakov, G. Morgenthal, Methods for flutter stability analysis of long-span bridges: a review, Proceedings of the Institution of Civil Engineers - Bridge Engineering, 170 (2017) 271-310. https://doi.org/10.1680/jbren.15.00039

[9]. F. Rizzo, L. Caracoglia, Artificial neural network model to predict the flutter velocity of suspension bridges, Computers & Structures, 233 (2020) 106236. https://doi.org/10.1016/j.compstruc.2020.106236

[10]. H. X. Nam, V. M. Trung, N. N. Son, N. N. Long, Vibration-based damage detection in cable-stayed bridges using a novel 1D-ConvNeXt-LSTM network, Transport and Communications Science Journal, 77 (2026) 485-499. https://doi.org/10.47869/tcsj.77.4.11

[11]. H. X. Nam, T. N. Hoa, B. T. Thanh, B. P. Loc, V. Q. Tuyen, A. Nguyen, A positional encoding-enhanced Kolmogorov-Arnold convolutional network for structural health monitoring, Structures, 89 (2026) 111970. https://doi.org/10.1016/j.istruc.2026.111970

[12]. N. L. M. Dang, H. X. Nam, V. M. Trung, N. K. N. Bao, Detection of damage in steel truss bridges using a hybrid 1DCNN-BIGRU model and time-series data augmentation techniques, Transport and Communications Science Journal, 76 (2025) 1281-1295 (in Vietnamese). https://doi.org/10.47869/tcsj.76.9.11

[13]. T. Canor, L. Caracoglia, V. Denoël, Application of random eigenvalue analysis to assess bridge flutter probability, Journal of Wind Engineering and Industrial Aerodynamics, 140 (2015) 79-86. https://doi.org/10.1016/j.jweia.2015.02.001

[14]. S. Arangio, F. Bontempi, Structural health monitoring of a cable-stayed bridge with Bayesian neural networks, Structure and Infrastructure Engineering, 11 (2015) 575-587. https://doi.org/10.1080/15732479.2014.951867

[15]. E. Cheynet, FlutterBridge_FD: the coupled flutter velocity of a single-span suspension bridge computed in the frequency domain. https://github.com/ECheynet/FlutterBridge_FD, 2023, (accessed 25/09/2026).

[16]. S. Liu, C. S. Cai, Y. Han, Time-domain simulations of turbulence effects on the aerodynamic flutter of long-span bridges, Advances in Bridge Engineering, 1 (2020) 7. https://doi.org/10.1186/s43251-020-00007-6

[17]. I. Khan, D. Shan, Q. Li, J. He, F. L. Nan, Data interpretation and continuous modal parameter identification of cable stayed bridge, The Open Civil Engineering Journal, 9 (2015) 577-591. https://doi.org/10.2174/1874149501509010577

[18]. H. Tran-Ngoc, S. Khatir, G. De Roeck, T. Bui-Tien, L. Nguyen-Ngoc, M. Abdel Wahab, Model updating for Nam O bridge using particle swarm optimization algorithm and genetic algorithm, Sensors, 18 (2018) 4131. https://doi.org/10.3390/s18124131

[19]. R. Storn, K. Price, Differential evolution - a simple and efficient heuristic for global optimization over continuous spaces, Journal of Global Optimization, 11 (1997) 341-359. https://doi.org/10.1023/A:1008202821328

[20]. M. D. McKay, R. J. Beckman, W. J. Conover, Comparison of three methods for selecting values of input variables in the analysis of output from a computer code, Technometrics, 21 (1979) 239-245. https://doi.org/10.1080/00401706.1979.10489755

[21]. C. E. Rasmussen, C. K. I. Williams, Gaussian Processes for Machine Learning, MIT Press, Cambridge, 2006.

[22]. L. Breiman, Random forests, Machine Learning, 45 (2001) 5-32. https://doi.org/10.1023/A:1010933404324

[23]. T. Chen, C. Guestrin, XGBoost: a scalable tree boosting system, in Proceedings of the 22nd ACM SIGKDD International Conference on Knowledge Discovery and Data Mining (San Francisco, 13-17/08/2016), 2016, ACM, 785-794. https://doi.org/10.1145/2939672.2939785

[24]. F. Pedregosa, G. Varoquaux, A. Gramfort, V. Michel, B. Thirion, O. Grisel, M. Blondel, P. Prettenhofer, R. Weiss, V. Dubourg, J. Vanderplas, A. Passos, D. Cournapeau, M. Brucher, M. Perrot, E. Duchesnay, Scikit-learn: machine learning in Python, Journal of Machine Learning Research, 12 (2011) 2825-2830.

[25]. A. Jain, N. P. Jones, R. H. Scanlan, Coupled flutter and buffeting analysis of long-span bridges, Journal of Structural Engineering, 122 (1996) 716-725. https://doi.org/10.1061/(ASCE)0733-9445(1996)122:7(716)

[26]. A. Šarkić, R. Fisch, R. Höffer, K.-U. Bletzinger, Bridge flutter derivatives based on computed, validated pressure fields, Journal of Wind Engineering and Industrial Aerodynamics, 104-106 (2012) 141-151. https://doi.org/10.1016/j.jweia.2012.02.033